Title
The Absence of DHHC3 Affects Primary and Latent Herpes Simplex Virus 1 Infection

Journal
Journal of Virology, 92(4)

ISSN
0022-538X

Authors
Wang, Shaohui
Mott, Kevin R
Cilluffo, Marianne
et al.

Publication Date
2018-02-15

DOI
10.1128/jvi.01599-17

Peer reviewed

AMERICAN SOCIETY FOR MICROBIOLOGY | Journal of Virology®

CELLULAR RESPONSE TO INFECTION

The Absence of DHHC3 Affects Primary and Latent Herpes Simplex Virus 1 Infection

Shaohui Wang,[a] Kevin R. Mott,[a] Marianne Cilluffo,[b] Casey L. Kilpatrick,[c] Shoko Murakami,[c] Alexander V. Ljubimov,[d] Konstantin G. Kousoulas,[e] Sita Awasthi,[f] Bernhard Luscher,[c] Homayon Ghiasi[a]

[a]Center for Neurobiology and Vaccine Development, Ophthalmology Research, Department of Surgery, Los Angeles, California, USA

[b]Brain Research Institute, UCLA, Los Angeles, California, USA

[c]Department of Biology, Biochemistry and Molecular Biology, and Psychiatry, Pennsylvania State University, University Park, Pennsylvania, USA

[d]Eye Program, Board of Governors Regenerative Medicine Institute, Cedars-Sinai Medical Center, and David Geffen School of Medicine, University of California Los Angeles, Los Angeles, California, USA

[e]Division of Biotechnology and Molecular Medicine, School of Veterinary Medicine, Louisiana State University, Baton Rouge, Louisiana, USA

[f]Infectious Disease Division, Department of Medicine, Perelman School of Medicine, University of Pennsylvania, Philadelphia, Pennsylvania, USA

ABSTRACT UL20, an essential herpes simplex virus 1 (HSV-1) protein, is involved in cytoplasmic envelopment of virions and virus egress. We reported recently that UL20 can bind to a host protein encoded by the zinc finger DHHC-type containing 3 (*ZDHHC3*) gene (also known as Golgi-specific DHHC zinc finger protein [GODZ]). Here, we show for the first time that HSV-1 replication is compromised in murine embryonic fibroblasts (MEFs) isolated from GODZ$^{-/-}$ mice. The absence of GODZ resulted in blocking palmitoylation of UL20 and altered localization and expression of UL20 and glycoprotein K (gK); the expression of gB and gC; and the localization and expression of tegument and capsid proteins within HSV-1-infected MEFs. Electron microscopy revealed that the absence of GODZ limited the maturation of virions at multiple steps and affected the localization of virus and endoplasmic reticulum morphology. Virus replication in the eyes of ocularly HSV-1-infected GODZ$^{-/-}$ mice was significantly lower than in HSV-1-infected wild-type (WT) mice. The levels of UL20, gK, and gB transcripts in the corneas of HSV-1-infected GODZ$^{-/-}$ mice on day 5 postinfection were markedly lower than in WT mice, whereas only UL20 transcripts were reduced in trigeminal ganglia (TG). In addition, HSV-1-infected GODZ$^{-/-}$ mice showed notably lower levels of corneal scarring, and HSV-1 latency reactivation was also reduced. Thus, normal HSV-1 infectivity and viral pathogenesis are critically dependent on GODZ-mediated palmitoylation of viral UL20.

IMPORTANCE HSV-1 infection is widespread. Ocular infection can cause corneal blindness; however, approximately 70 to 90% of American adults exposed to the virus show no clinical symptoms. In this study, we show for the first time that the absence of a zinc finger protein called GODZ affects primary and latent infection, as well as reactivation, in ocularly infected mice. The reduced virus infectivity is due to the absence of the GODZ interaction with HSV-1 UL20. These results strongly suggest that binding of UL20 to GODZ promotes virus infectivity *in vitro* and viral pathogenesis *in vivo*.

KEYWORDS knockout, GODZ, latency reactivation, primary infection, EM, zinc finger protein, HSV-1, TG, zinc finger protein, latency

Received 8 September 2017 **Accepted** 15 November 2017

Accepted manuscript posted online 29 November 2017

Citation Wang S, Mott KR, Cilluffo M, Kilpatrick CL, Murakami S, Ljubimov AV, Kousoulas KG, Awasthi S, Luscher B, Ghiasi H. 2018. The absence of DHHC3 affects primary and latent herpes simplex virus 1 infection. J Virol 92:e01599-17. https://doi.org/10.1128/JVI.01599-17.

Editor Jae U. Jung, University of Southern California

Address correspondence to Homayon Ghiasi, ghiasih@cshs.org.

The herpes simplex virus 1 (HSV-1)-encoded protein UL20 is essential for cytoplasmic envelopment of virions and virus egress. UL20 has been shown to interact with HSV-1 glycoprotein K (gK) (1), and both UL20 and gK are classified as essential genes for HSV-1 infectivity (1–5). We found recently that UL20 binds to GODZ (Golgi-specific DHHC zinc finger protein)/DHHC3, a member of the Asp-His-His-Cys (DHHC) family of palmitoyl transferases (6). These enzymes are characterized by a conserved DHHC motif embedded within a larger conserved cysteine-rich domain (7–9). Members of the DHHC family are present in all eukaryotes (10, 11) and are highly conserved (12). To date, 23 different *DHHC* genes have been identified in humans and mice (9–11, 13). Proteins containing the DHHC motif have been shown to act as *S*-palmitoyl transferases (14). As *S*-palmitoylation is readily reversible, this posttranslational protein modification can potentially play a regulatory role in functions that rely on protein-membrane interactions (15–17).

GODZ is localized predominately within the *cis*-Golgi complex (12, 18, 19) and has been shown to be involved in the palmitoylation of several proteins, especially in neurons (18–22). Using a dominant-negative construct of GODZ to characterize its role in virus infectivity *in vitro*, we have shown that the interaction of UL20 with GODZ is required for optimal virus infectivity, that UL20 is palmitoylated by GODZ in cultured cells, and that this palmitoylation is required for virus infectivity (6).

We recently generated a mouse strain lacking GODZ expression (19). Characterization of these GODZ$^{-/-}$ mice confirmed that palmitoylation of the γ2 subunit of $GABA_A$ receptors and of a second substrate, a growth-associated protein of 43 kDa that is involved in trafficking of $GABA_A$ receptors, was significantly reduced in the brains of GODZ$^{-/-}$ mice compared to wild-type (WT) mice. In the present study, we investigated the roles of GODZ in HSV-1 infectivity using GODZ$^{-/-}$ mice and mouse embryonic fibroblasts (MEFs) derived from these mice. We show for the first time that (i) the absence of GODZ in MEFs affected virus infectivity, UL20 palmitoylation, and UL20 and gK subcellular localization, as documented using a combination of plaque assays, immunofluorescence staining (IF), fluorescence-activated cell sorting (FACS), Western blotting, and electron microscopy (EM); (ii) in the eyes and trigeminal ganglia (TG) of GODZ$^{-/-}$ mice, HSV-1 infectivity was lower during primary infection than in WT mice; and (iii) the absence of GODZ affected normal trafficking of UL20 through the Golgi network and significantly reduced latency reactivation and corneal scarring (CS) in ocularly infected mice compared with WT mice.

RESULTS

HSV-1 replication is reduced in *GODZ*$^{-/-}$ MEFs. To test if the absence of GODZ affects HSV-1 replication, we infected MEFs from GODZ$^{-/-}$ and WT mice with 0.01, 0.1, and 1 PFU/cell of HSV-1 strain McKrae for 12, 24, 48, and 72 h. The kinetics of virus replication were determined using a standard plaque assay on RS (rabbit skin) cells (Fig. 1). Compared with infected MEFs from WT mice, GODZ$^{-/-}$ MEFs had significantly lower virus titers at 48 and 72 h postinfection (p.i.) using 0.01 PFU/cell (Fig. 1A). GODZ$^{-/-}$ MEFs infected with 0.1 PFU/cell (Fig. 1B) and 1 PFU/cell (Fig. 1C) showed lower virus replication at 24, 48, and 72 h p.i. than identically treated WT MEFs. The greater differences in virus titers observed in GODZ$^{-/-}$ versus WT MEFs at 1 PFU/cell compared with smaller differences at 0.01 and 0.1 PFU/cell could be due to faster responses to higher doses of infection in GODZ$^{-/-}$ MEFs. Alternatively, it could take longer to detect differences between GODZ$^{-/-}$ and WT MEFs at lower doses of infection.

To corroborate these results, we infected WT and GODZ$^{-/-}$ MEFs with 0.1 and 1 PFU/cell of green fluorescent protein (GFP)-tagged HSV-1 (HSV-GFP$^+$) or 1 PFU/cell of HSV-1 strain McKrae and used FACS and immunostaining to determine the expression of GFP and HSV-1 gC (Fig. 2A to E), respectively. After infection with HSV-GFP$^+$ at 0.1 PFU/cell (Fig. 2A) or 1 PFU/cell (Fig. 2B), there were markedly fewer GFP$^+$ GODZ$^{-/-}$ MEFs than GFP$^+$ WT MEFs. FACS analysis of the percentages of GFP$^+$ cells confirmed a lower percentage of GFP$^+$ GODZ$^{-/-}$ MEFs than GFP$^+$ WT MEFs, independent of the dose of infection (0.6% versus 2% at 0.1 PFU/cell and 6% versus 14% at 1 PFU/cell)

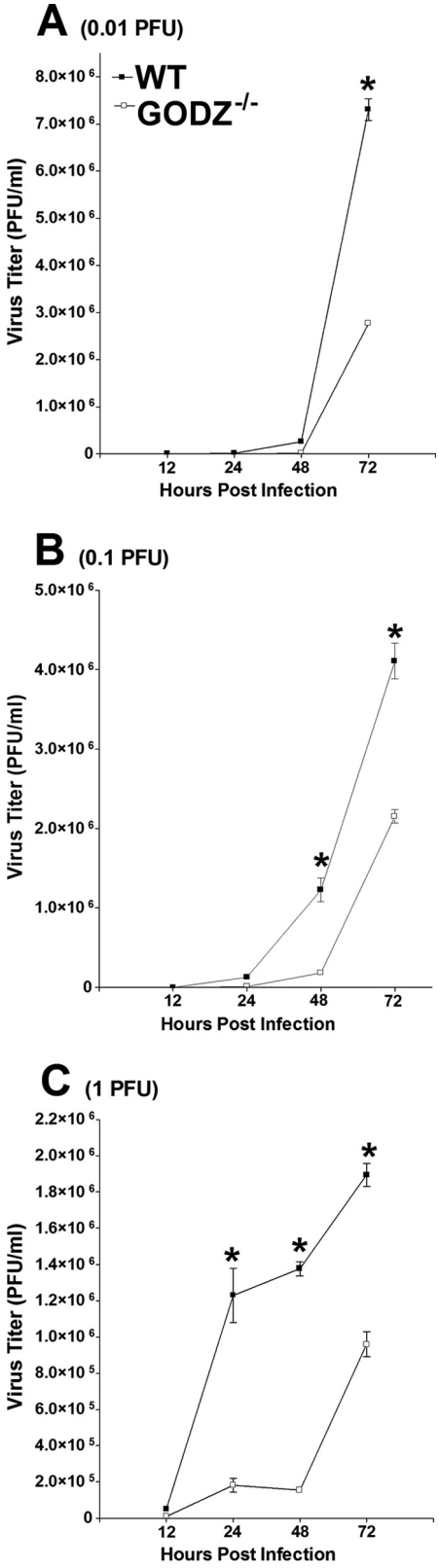

FIG 1 Virus replication in MEFs. Subconfluent MEF monolayers from WT and GODZ$^{-/-}$ mice were infected with 0.01 (A), 0.1 (B), or 1 (C) PFU/cell of McKrae virus for 12, 24, 48, and 72 h. Total virus was harvested at the indicated times postinfection by two cycles of freeze-thawing. The amount of virus at each time for each cell was determined by standard plaque assays on RS cells. Each point represents the mean titer ± standard error of the mean (SEM) from 5 independent experiments. *, significant differences between the two groups using the Student *t* test.

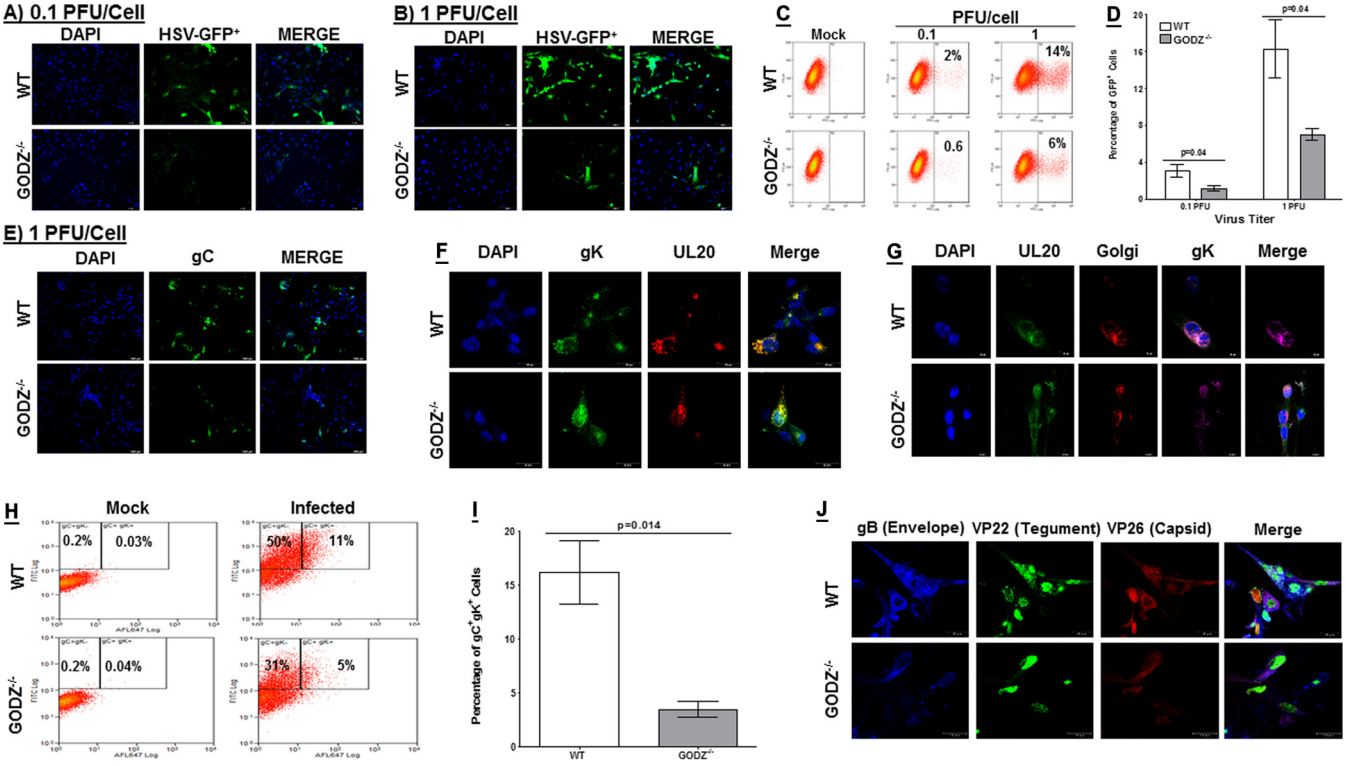

FIG 2 Infection of MEFs with HSV-GFP$^+$, McKrae, or VC1 virus. (A and B) Detection of HSV-GFP$^+$ cells by IF. Subconfluent MEF cultures from WT and GODZ$^{-/-}$ mice were infected with 0.1 (A) or 1 (B) PFU/cell of HSV-GFP$^+$ virus for 24 h, and infected cells were processed as described in Materials and Methods. The photomicrographs are shown at ×20 direct magnification. (C) Detection of HSV-GFP$^+$ cells by FACS. MEFs from WT and GODZ$^{-/-}$ mice were infected as for panels A and B. The cells were trypsinized and fixed, and the presence of GFP$^+$ cells for each PFU was determined by FACS. (D) Quantitation of HSV-GFP$^+$ cells by FACS. Percentages of GFP$^+$ cells treated as for panel C were quantitated by FACS. Each point represents the mean ± SEM from three independent experiments. (E) Detection of HSV-gC by IF. Subconfluent MEF cultures from WT and GODZ$^{-/-}$ mice grown on LabTek chamber slides were infected with 1 PFU/cell of McKrae virus for 16 h. The slides were fixed and stained with anti-gC antibody (green) and DAPI nuclear stain (blue). (F) Detection of UL20 and gK by IF in VC1-infected cells. Subconfluent MEF cultures from WT and GODZ$^{-/-}$ mice were infected with 2 PFU/cell of VC1 virus for 24 h. The slides were stained with anti-V5 (green; for detection of gK), anti-FLAG (red; for detection of UL20), and DAPI nuclear stain (blue). (G) Detection of UL20, gK, and GM130 by IF in VC1-infected cells. Subconfluent MEF cultures from WT and GODZ$^{-/-}$ mice were infected with 2 PFU/cell of VC1 virus for 16 h. The slides were stained with anti-FLAG (green; for detection of UL20), anti-GM130 (red; a Golgi complex marker), anti-V5 (purple; for detection of gK), and DAPI nuclear stain (blue). Colocalization is visualized as pink in the merged images. The photomicrographs are shown at ×630 direct magnification. (H) Detection of cell surface expression of gC and gK by FACS in VC1-infected cells. MEFs from WT and GODZ$^{-/-}$ mice were infected with 1 PFU/cell of VC1 virus for 24 h or mock infected as described above. The cells were trypsinized, stained with anti-gC and anti-V5 (for detection of gK), washed, and fixed. Percentages of gC$^+$ gK$^+$ and gC$^+$ gK$^-$ cells were determined by FACS. (I) Quantitation of gC$^+$ gK$^+$ cells by FACS. Percentages of gC$^+$ gK$^+$ cells treated as for panel H were quantitated by FACS. Each point represents the mean ± SEM from three independent experiments. (J) Infection of MEFs with YK608 virus. Subconfluent MEF cultures from WT and GODZ$^{-/-}$ mice were infected with 2 PFU/cell of YK608 virus for 16 h. The confocal photomicrographs are shown at ×630 direct magnification.

(Fig. 2C). There was a significant reduction in the number of HSV-GFP$^+$ cells in the infected GODZ$^{-/-}$ MEFs than in infected WT MEFs at both 0.1 and 1 PFU of GFP$^+$ HSV-1 (Fig. 2D) ($P = 0.04$). We next infected MEFs from GODZ$^{-/-}$ and WT mice with 1 PFU/cell of HSV-1 strain McKrae and incubated the infected cells with anti-HSV-1 gC antibody. Immunostaining showed that the percentage of HSV-1 gC$^+$ cells was markedly lower in GODZ$^{-/-}$ than in WT MEFs (Fig. 2E). Collectively, these results indicate that efficient replication of HSV-1 in MEFs is dependent on GODZ of host cells.

Subcellular localization of UL20 and gK is altered in HSV-1-infected *GODZ*$^{-/-}$ MEFs. We have demonstrated previously that UL20 binds to both GODZ (6) and HSV-1 gK (23). In addition, we found that overexpression of a dominant-negative mutant of GODZ (GODZ^{C157S}) affected UL20 and gK expression and localization *in vitro* (6). As utilization of dominant-negative mutant approaches to analysis of function can be problematic, we determined the expression of UL20 and gK, and their interaction, in HSV-1-infected GODZ$^{-/-}$ MEFs. To facilitate analysis, we utilized an HSV-1 strain, VC1, that has been engineered to express UL20 and gK tagged with 3×FLAG and a V5 epitope, respectively (24). MEFs from WT and GODZ$^{-/-}$ mice were infected with VC1 virus (1 PFU/cell). At 24 h p.i., the cells were fixed and permeabilized, followed by

immunostaining with anti-V5 (to detect gK) and anti-FLAG (to detect UL20) antibodies (Fig. 2F). Immunofluorescent staining confirmed that in the infected WT MEFs, gK and UL20 expression was localized mostly at the cell surface and in the cytoplasm (Fig. 2F, WT). Furthermore, UL20 and gK were colocalized in infected WT MEFs (Fig. 2F, WT, Merge). In contrast, in MEFs from GODZ$^{-/-}$ mice, gK and UL20 were localized predominantly within and around nuclei (Fig. 2F, GODZ$^{-/-}$). The effect was more pronounced for UL20, which retained some colocalization with gK within the infected cells (Fig. 2F, GODZ$^{-/-}$, Merge). Thus, the absence of GODZ expression affected the intracellular localization of both UL20 and gK in infected MEFs.

It is well established that GODZ is a Golgi complex protein (12, 18, 19), and binding of GODZ with UL20 has been shown to occur within the Golgi complex (6). We therefore infected MEFs from WT and GODZ$^{-/-}$ mice with VC1 virus for 16 h and then fixed and permeabilized the infected cells prior to incubation with anti-GM130 (to detect the Golgi complex), as well as anti-FLAG (to detect UL20) and anti-V5 (to detect gK) antibodies (Fig. 2G). As described above (Fig. 2F), in the infected WT MEFs, most UL20 (Fig. 2G, UL20) and gK (Fig. 2G, gK) expression was extranuclear (Fig. 2G, WT). In these cells, there was extensive colocalization of both UL20 and gK with GM130 (Fig. 2G, WT, Merge). The intensity of expression of all three proteins was significantly lower in the infected GODZ$^{-/-}$ MEFs than in the infected WT cells (Fig. 2G, compare WT with GODZ$^{-/-}$). In GODZ$^{-/-}$ MEFs (Fig. 2G, GODZ$^{-/-}$), UL20 and gK were again localized primarily in and around the nucleus. The absence of GODZ did not appear to affect the localization of GM130 in the cytoplasm of the MEFs, and merging of the channels showed some colocalization of UL20 and gK with GM130 within the infected GODZ$^{-/-}$ cells (Fig. 2G, GODZ$^{-/-}$, Merge).

We next compared the cell surface expression of gK and gC in MEFs from WT and GODZ$^{-/-}$ mice that were infected *in vitro* with VC1 virus for 24 h. Unfixed, nonpermeabilized live MEFs were incubated with anti-V5 and anti-HSV-1 gC antibodies, and the cell surface expression of gK and gC was examined by FACS analysis (Fig. 2H). Approximately 50% of infected WT MEFs were gC^{+} gK^{-} versus 31% of infected GODZ$^{-/-}$ MEFs. Similarly, 11% of infected WT cells were gC^{+} gK^{+} versus 5% of infected GODZ$^{-/-}$ MEFs (Fig. 2H, Infected). As expected, the mock-infected groups did not show significant numbers of positive cells (Fig. 2H, Mock). These results suggest that the absence of GODZ affects the cell surface expression of both gK and gC in infected MEFs. The lower percentage of gK-positive cells was most likely due to the lower copy number of *gK* than of *gC* in infected cells, as we reported previously (25). Quantification of the gC^{+} gK^{+} cells from three separate FACS analyses of infected cells revealed a significant reduction in HSV-1 signal in GODZ$^{-/-}$ compared to WT MEFs (Fig. 2I) ($P = 0.014$). The above-mentioned results using a combination of plaque assays, FACS, and IF suggest that GODZ is required for normal virus replication and for normal subcellular localization of UL20 and gK, but not gC.

HSV-1 strain McKrae virion formation is disrupted in infected *GODZ*$^{-/-}$ MEFs. HSV-1 consists of a nucleocapsid that is coated with a layer of tegument proteins and enclosed in a layer of envelope proteins (26). Potentially, the absence of GODZ-mediated palmitoylation could disrupt this structure. To assess the expression and localization of representatives of each of these three categories of proteins, we used a recombinant HSV-1 encoding nucleocapsid (VP26), tegument (VP22), and envelope (gB) proteins that were tagged to enable their localization directly without antibody staining (27). MEFs from WT and GODZ$^{-/-}$ mice were grown on LabTek slides and infected with 2 PFU/cell of the YK608 virus, and the infected cells were examined by confocal microscopy at 16 h p.i. (Fig. 2J). In the infected WT MEFs, the intensity of gB envelope protein staining was high and was localized mainly in the cytoplasm and around the nucleus (Fig. 2J, gB, WT), whereas in the infected GODZ$^{-/-}$ MEFs, the intensity of gB staining was very weak, and it was mainly seen in the cytoplasm (Fig. 2J, compare gB, GODZ$^{-/-}$, with gB, WT). In infected WT MEFs, the VP22 tegument protein was localized mainly in the cytoplasm (Fig. 2J, VP22, WT), whereas its distribution in infected MEFs from GODZ$^{-/-}$ mice was more nuclear, and its expression was significantly lower than

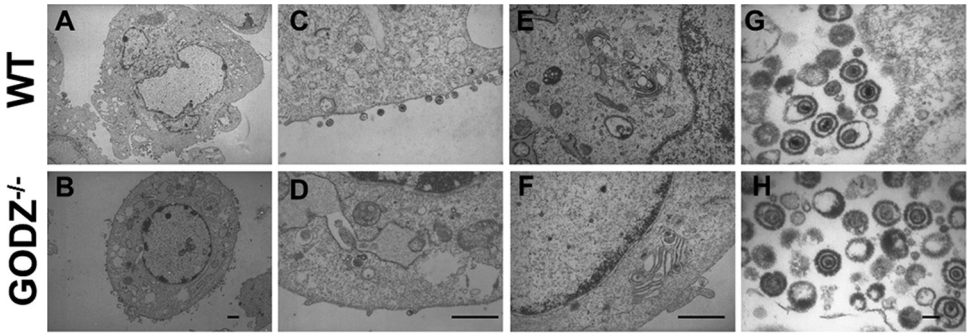

FIG 3 Electron micrographs of WT and GODZ$^{-/-}$ MEFs infected with HSV-1 strain McKrae. Subconfluent MEF monolayers from WT and GODZ$^{-/-}$ mice were infected with 1 PFU/cell of HSV-1 strain McKrae for 24 h. The cells were prepared for transmission electron microscopy as described in Materials and Methods. Scale bars, 1 μm (A to F) and 0.1 μm (G and H).

in the infected WT MEFs (Fig. 2J, VP22, compare WT with GODZ$^{-/-}$). The VP26 capsid protein in infected WT cells was distributed in both the cytoplasm and the nucleus and was detected in granular structures within the nucleus (Fig. 2J, VP26, WT). In contrast, VP26 was retained in the nuclei of infected GODZ$^{-/-}$ MEFs (Fig. 2J, VP26, compare WT with GODZ$^{-/-}$). Merged images showed that gB and VP22 colocalized with each other but not with VP26 in both the infected WT and GODZ$^{-/-}$ cells (Fig. 2J, Merge). Thus, GODZ is required for normal subcellular localization of gB, VP22, and VP26.

To further examine the role of GODZ in virion formation, WT and GODZ$^{-/-}$ MEFs were infected with 1 PFU/cell of HSV-1 strain McKrae, harvested at 24 h postinfection, and analyzed by transmission electron microscopy (Fig. 3). A substantially greater number of extracellular virion particles were detected in WT than in GODZ$^{-/-}$ cells (Fig. 3A versus B and C versus D). A higher density of intracellular virion capsids was visualized within the nuclei of GODZ$^{-/-}$ cells than in those of WT cells (Fig. 3A versus B). The cellular membranes of the GODZ$^{-/-}$ cells appeared less smooth and had multiple breaks in comparison to those of the infected WT MEFs (not shown). The infected GODZ$^{-/-}$ cells contained numerous cytoplasmic vacuoles, some of which contained immature virion particles, and the endoplasmic reticulum (ER) appeared more swollen than that of infected WT cells (Fig. 3A versus B). Furthermore, virions were found within the Golgi apparatus in MEFs from GODZ$^{-/-}$ mice (Fig. 3F), and more empty virions were detected in GODZ$^{-/-}$ MEFs (Fig. 3H) versus WT MEFs (Fig. 3G). Although necrotic cells were present in both the infected WT and GODZ$^{-/-}$ cells, more necrotic cells were observed in the GODZ$^{-/-}$ cells. These necrotic cells were characterized by swollen mitochondria, diffuse cytoplasm, and breaks in the plasma membrane. The nuclear membranes of infected GODZ$^{-/-}$ MEFs appeared swollen and enlarged compared to those of the infected WT MEFs (Fig. 3B versus A).

Absence of UL20 palmitoylation in infected GODZ$^{-/-}$ MEFs. Recently, using two-hybrid and pulldown assays, we demonstrated that UL20, but no other HSV-1 gene-encoded proteins, binds specifically to GODZ (6). In addition, using a catalytically inactive dominant-negative GODZ construct, we showed that GODZ is involved in palmitoylation of UL20. To assess whether UL20 palmitoylation was impaired in GODZ$^{-/-}$ MEFs, similarly to cells transfected with dominant-negative GODZ, GODZ$^{-/-}$ and WT MEFs were infected with 1 PFU/cell of VC1 virus or mock infected, and palmitoylation was analyzed using the acyl biotin exchange method as described in Materials and Methods. Western blots of UL20 revealed no changes in palmitoylation of UL20 in infected GODZ$^{-/-}$ MEFs in the presence (Fig. 4, top, lane 4) or in the absence (Fig. 4, top, lane 3) of hydroxylamine (HAM). In contrast, UL20 from VC1-infected WT MEFs showed a stronger band in the presence of HAM (Fig. 4, top, lane 2) than in the absence of HAM (Fig. 4, lop, lane 1). Overall, there was a dramatic reduction in palmitoylated UL20 in infected GODZ$^{-/-}$ MEFs (Fig. 4, top, lane 4) compared with infected MEFs from WT mice (Fig. 4, top, lane 2). No palmitoylated band was detected

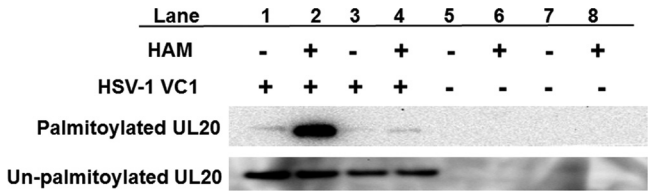

FIG 4 UL20 is not palmitoylated in MEFs derived from GODZ$^{-/-}$ mice. MEFs from GODZ$^{-/-}$ and WT mice were infected with 1 PFU/cell of VC1 virus or mock infected. At 24 h p.i., cells were harvested, and palmitoylation of UL20 was determined as described in Materials and Methods. (Top) Lanes: 1, VC1-infected MEFs from WT mice without HAM treatment; 2, VC1-infected MEFs from WT mice with HAM treatment; 3, VC1-infected MEFs from GODZ$^{-/-}$ mice without HAM treatment; 4, VC1-infected MEFs from GODZ$^{-/-}$ mice with HAM treatment; 5, mock-infected control MEFs from WT mice without HAM treatment; 6, mock-infected control MEFs from WT mice with HAM treatment; 7, mock-infected control MEFs from GODZ$^{-/-}$ mice without HAM treatment; 8, mock-infected control MEFs from GODZ$^{-/-}$ mice with HAM treatment. (Bottom) Detection of UL20 bands in all four VC1-infected MEFs (lanes 1 to 4), but not in mock-infected control MEFs (lanes 5 to 8). Experiments were repeated 4 times.

in mock-infected MEFs from WT (Fig. 4, top, lanes 5 and 6) or GODZ$^{-/-}$ (Fig. 4, top, lanes 7 and 8) mice in the presence or in the absence of HAM. The presence of UL20 in VC1-infected lanes was confirmed by stripping the upper filter of horseradish peroxidase (HRP)-conjugated streptavidin, followed by probing of the membrane with anti-FLAG antibody and HRP-conjugated secondary antibody (Fig. 4, bottom). The UL20 band was detected in all treatment groups irrespective of the presence or the absence of HAM. Thus, our results suggest that palmitoylation of UL20 is GODZ dependent.

Clearance of HSV-1 is faster in the eyes of ocularly infected *GODZ*$^{-/-}$ mice. To determine if the absence of GODZ affected the rate of clearance of infectious virus from HSV-1-infected eyes, GODZ$^{-/-}$ and WT control mice were ocularly infected with HSV-1 strain McKrae. Tear films were collected from 40 eyes/group on days 1, 2, 3, 4, 5, 6, and 7 p.i., and the presence of infectious virus was determined by plaque assays (Fig. 5). Between days 1 and 5 p.i., the amounts of infectious virus in the eyes of WT mice were significantly higher than in the eyes of infected GODZ$^{-/-}$ mice (Fig. 5); however, the virus titers in the eyes of the two groups of infected mice were similar on days 6 and

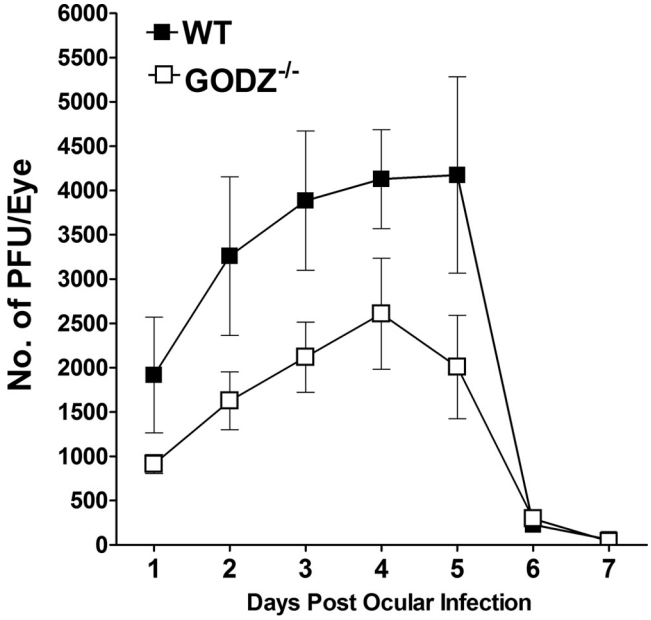

FIG 5 Virus titers in the eyes of infected mice. WT and GODZ$^{-/-}$ mice were ocularly infected with 2×10^5 PFU/eye of McKrae virus as described in Materials and Methods. Tear films were collected on days 1 to 7, and virus titers were determined by standard plaque assays. Each point represents the mean titers ± SEM of 40 eyes from two separate experiments.

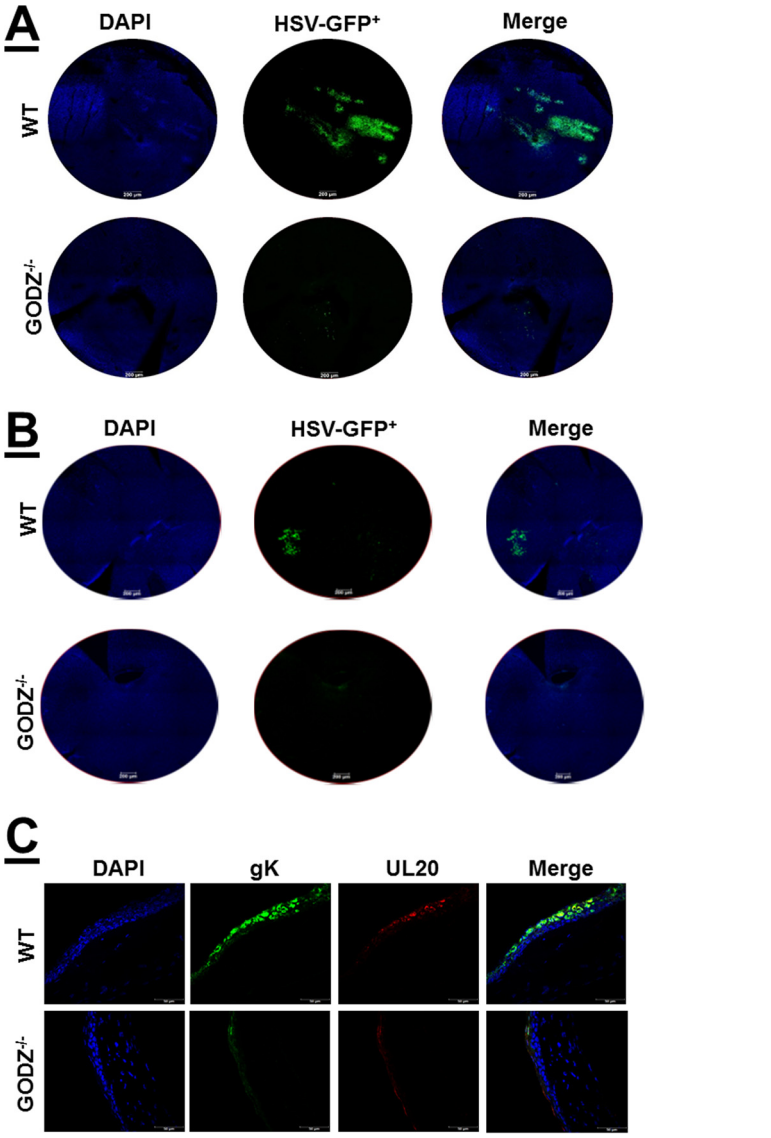

FIG 6 Infection of mice with HSV-GFP$^+$ and VC1 viruses. (A and B) Detection of GFP in the corneas of infected mice. Corneas from WT and GODZ$^{-/-}$ mice were scarified before ocular infection and then were infected with 2×10^5 PFU/eye of HSV-GFP$^+$ virus. On days 4 (A) and 7 (B) p.i., whole corneas from HSV-GFP$^+$-infected mice were excised as described in Materials and Methods. The presence of HSV-1-infected GFP$^+$ cells was assessed by microscopy. (C) Detection of UL20 and gK in corneas of VC1-infected mice by IF. Corneas from WT and GODZ$^{-/-}$ mice were scarified before ocular infection and infected with 2×10^5 PFU/eye of VC1 virus. The eyes were removed from each animal on day 5 p.i. and sectioned, and the slides were fixed and stained with anti-V5 (green; for detection of gK), anti-FLAG (red; for detection of UL20), and DAPI nuclear stain (blue). The images were acquired using confocal microscopy, and colocalization is visualized as yellow in the merged images. The photomicrographs are shown at ×630 direct magnification.

7 p.i. (Fig. 5). Thus, the absence of GODZ interaction in the GODZ$^{-/-}$ mice appeared to reduce virus replication in the eyes of infected mice.

We next infected GODZ$^{-/-}$ and WT mice with HSV-GFP$^+$ following corneal scarification. On days 4 and 7 p.i., we compared the densities of GFP$^+$ cells in corneal whole mounts from infected GODZ$^{-/-}$ and WT mice (Fig. 6A and B). On day 4 p.i., the numbers of GFP$^+$ cells present in the corneas from GODZ$^{-/-}$ mice were markedly lower than the numbers of GFP$^+$ cells in the corneas from infected WT mice (Fig. 6A, compare WT and GODZ$^{-/-}$). As expected from IF, the GFP$^+$ signal was lower on day 7 than on day 4 p.i., but the WT mice still had more GFP$^+$ cells than the GODZ$^{-/-}$ mice

(Fig. 6B, compare WT and GODZ$^{-/-}$). Together, these results showed lower HSV-1 infectivity in the corneas of the GODZ$^{-/-}$ mice than in those of the WT mice.

Our *in vitro* studies with MEFs had suggested that the absence of GODZ affected the localization of both UL20 and gK. Thus, we examined whether a similar effect could be observed in the corneas of HSV-1-infected GODZ$^{-/-}$ mice. Following corneal scarification, WT and GODZ$^{-/-}$ mice were ocularly infected with the VC1 virus. At day 5 p.i., eyes from infected mice were isolated, sectioned, and fixed prior to staining with anti-V5 and anti-FLAG antibodies (Fig. 6C). In the WT corneas, significant amounts of both gK (Fig. 6C, gK, WT) and UL20 (Fig. 6C, UL20, WT) were detected in the epithelia of infected corneas, and most of the gK and UL20 were colocalized (Fig. 6C, Merge, WT). In contrast, the levels of both gK and UL20 expression were markedly lower in the corneas of the infected GODZ$^{-/-}$ mice, with only a few gK-positive (Fig. 6C, gK, GODZ$^{-/-}$) and UL20-positive (Fig. 6C, UL20, GODZ$^{-/-}$) cells (Fig. 6C, Merge, GODZ$^{-/-}$), and the colocalization was too low to detect. Thus, similar to the results generated through analysis of MEFs *in vitro*, the absence of GODZ resulted in reduced accumulation and altered intracellular localization of UL20 and gK in the corneas of ocularly infected mice.

The expression of UL20, gK, and gB is altered during primary ocular infection of *GODZ*$^{-/-}$ mice. To investigate if the absence of GODZ affects the levels of viral transcripts *in vivo*, GODZ$^{-/-}$ and WT mice were infected with 2×10^5 PFU/eye of HSV-1 strain McKrae. The corneas and TG were collected on days 3, 5, and 7 p.i., and total RNA was isolated and subjected to TaqMan real-time (RT)-PCR to determine the copy numbers for UL20, gK, and gB mRNAs. GAPDH (glyceraldehyde-3-phosphate dehydrogenase) mRNA in each sample was used as an internal control. The results showed differences in the levels of each transcript in the corneas of infected GODZ$^{-/-}$ and WT mice (Fig. 7). On day 3 p.i., the levels of UL20 (Fig. 7A), gK (Fig. 7B), and gB (Fig. 7C) transcripts were similar in corneas of infected GODZ$^{-/-}$ and WT mice ($P > 0.05$). By day 5 p.i., the levels of UL20 (Fig. 7A), gK (Fig. 7B), and gB (Fig. 7C) transcripts in the corneas of the infected GODZ$^{-/-}$ mice and infected WT mice had increased compared with day 3 p.i.; however, the levels of all three transcripts in infected GODZ$^{-/-}$ mice were significantly lower than in infected WT mice ($P < 0.001$). On day 7 p.i., the levels of all three transcripts in both strains of mice has decreased and there was no statistically significant difference between the strains (Fig. 7A, B, and C) ($P > 0.05$).

Analysis of the TG of the infected mice indicated that the levels of UL20 were similar to those seen in the corneas (compare Fig. 7A with D). On day 3 p.i., the level of UL20 expression in infected GODZ$^{-/-}$ mice was similar to that in WT mice (Fig. 7D) ($P > 0.05$), but by day 5 p.i., it was significantly lower (Fig. 7D) ($P < 0.001$). By day 7 p.i., the levels of UL20 transcripts had declined in both infected GODZ$^{-/-}$ and WT mice, and there was no significant difference between the two groups (Fig. 7D) ($P > 0.05$). There were, however, no significant differences in the levels of gK (Fig. 7E) or gB (Fig. 7F) transcripts in the TG of infected GODZ$^{-/-}$ and WT mice on day 3, 5, or 7 p.i. ($P > 0.05$). In both the corneas and TG, the levels of gB transcripts were significantly higher than the levels of gK transcripts, and both were higher than the levels of UL20.

Collectively, these results indicated that the absence of GODZ affected UL20 transcription in a time-dependent and tissue-dependent manner, whereas gK and gB transcription were affected in a time-dependent but tissue-specific manner.

Corneal scarring is reduced in GODZ$^{-/-}$ mice ocularly infected with HSV-1. To determine if the absence of GODZ in mice with a C57BL/6J background, which are normally refractory to HSV-1 infection, affects the survival of the mice, WT and GODZ$^{-/-}$ mice were infected ocularly with HSV-1 strain McKrae. In multiple experiments, 4 out of 50 infected GODZ$^{-/-}$ mice died because of ocular infection (not shown). There was no statistically significant difference between the mortality of HSV-1-infected GODZ$^{-/-}$ mice and that of C57BL/6J WT controls ($P > 0.05$; Fisher's exact test). Corneal scarring was evaluated in surviving mice on day 28 post-ocular infection. There was significantly less corneal scarring in the GODZ$^{-/-}$ mice than in the

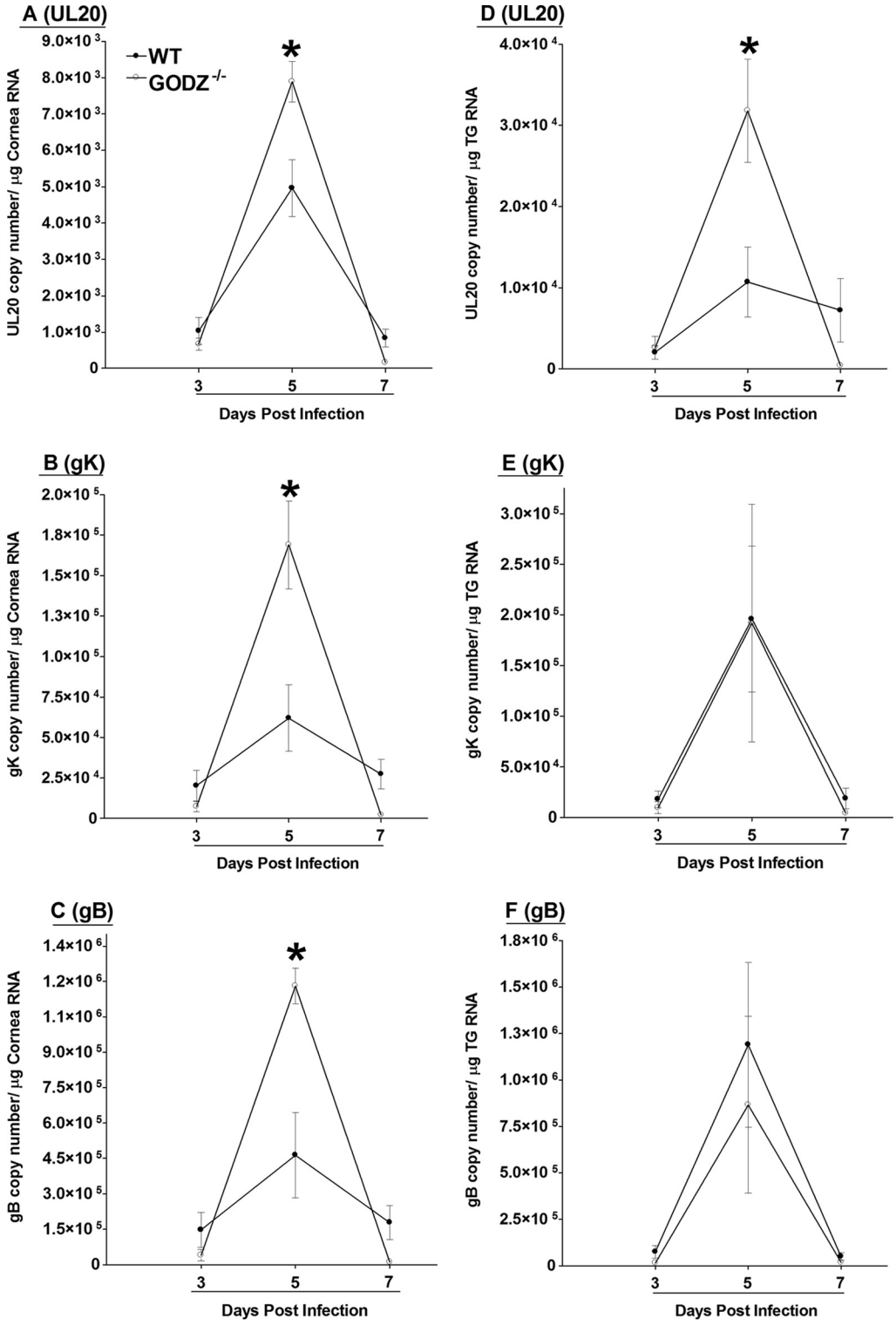

FIG 7 Expression of UL20, gK, and gB transcripts in corneas and TG of ocularly infected mice. WT and GODZ$^{-/-}$ mice were ocularly infected with 2×10^5 PFU/eye of McKrae virus. The levels of UL20, gK, and gB transcripts in the corneas and TG were determined on days 3, 5, and 7 p.i. by qRT-PCR. In each experiment, an estimated relative copy number of the HSV-1 UL20, gK, and gB was calculated using standard curves generated from pUL20 (6), pAC-gB1 (63), and pAc-gK1 (33). Briefly, the DNA template was serially diluted 10-fold so that 5 μl contained from 10^3 to 10^{11} copies of each plasmid and then subjected to TaqMan PCR with the same set of primers. By comparing the normalized threshold cycle of each sample to the threshold cycle of the standard, the copy number for each reaction was determined. GAPDH expression was used to normalize the relative expression of each transcript in corneas and TG of infected mice. Shown are the means $\pm$ SEM from 6 corneas or TG. (A) UL20 transcript in corneas. (B) gK transcript in corneas. (C) gB transcript in corneas. (D) UL20 transcript in TG. (E) gK transcript in TG. (F) gB transcript in TG.

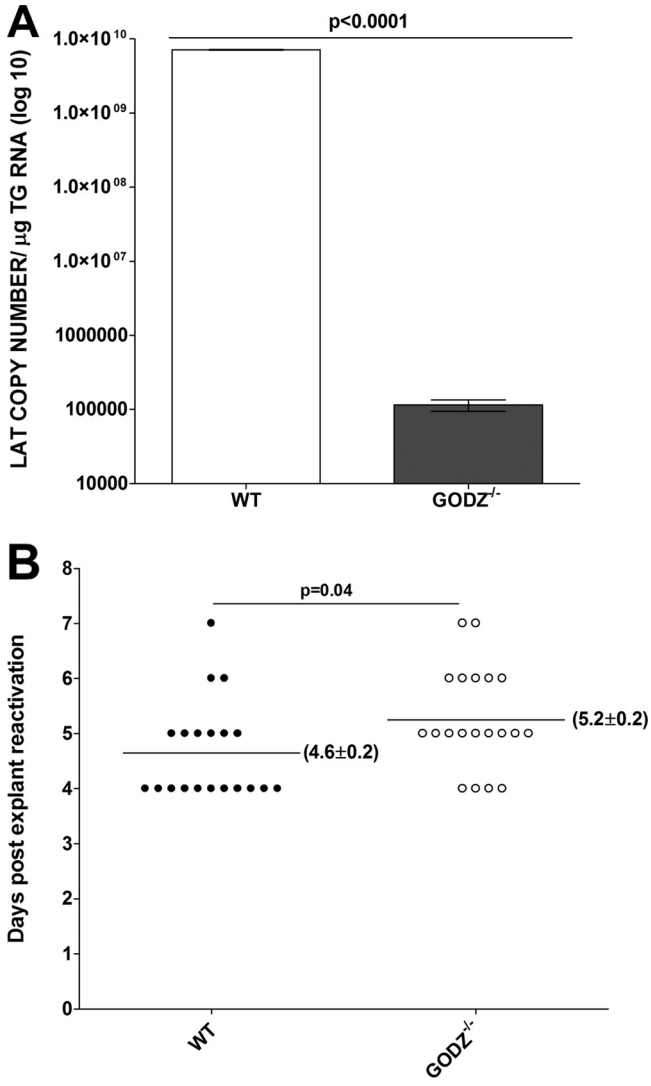

FIG 8 Levels of latency and durations of explant reactivation in ocularly infected mice. WT and GODZ$^{-/-}$ mice were ocularly infected with 2×10^5 PFU/eye of McKrae virus as described for Fig. 6. On day 28 p.i., TG from infected mice were harvested for qRT-PCR and explant reactivation. (A) Quantitation of LAT RNA in TG of latently infected mice. qRT-PCR was performed on each individual mouse TG. In each experiment, an estimated relative copy number of the HSV-1 LAT for viral RNA was calculated using standard curves generated from pGem5317. Briefly, the DNA template was serially diluted 10-fold so that 5 μl contained from 10^3 to 10^{11} copies of LAT and then subjected to TaqMan PCR with the same set of primers. By comparing the normalized threshold cycle of each sample to the threshold cycle of the standard, the copy number for each reaction was determined. GAPDH expression was used to normalize the relative expression of LAT RNA in the TG. Each point represents the mean ± SEM from 20 TG. (B) Explant reactivation in latent TG. Each individual TG from infected mice on day 28 p.i. was incubated in 1.5 ml of tissue culture medium at 37°C, and the presence of infectious virus was monitored for 15 days. For each virus, 20 TG from 10 mice were used. The average time that the TG from each group first showed CPE ± SEM is shown.

WT mice (see Fig. S1 in the supplemental material) ($P = 0.004$; Student's t test). Thus, the absence of GODZ reduced HSV-1-induced corneal scarring.

Latency reactivation is reduced in the TG of latently infected GODZ$^{-/-}$ mice. To measure latency, WT and GODZ$^{-/-}$ mice were infected ocularly with 2×10^5 PFU/eye of HSV-1 strain McKrae, and individual TG from the surviving mice were isolated on day 28 p.i. Total RNA was isolated, and TaqMan quantitative RT-PCR (qRT-PCR) was used to quantify latency-associated transcript (LAT) RNA levels. Cellular GAPDH DNA was used as an internal control. The amount of LAT RNA during latency in *GODZ*$^{-/-}$ mice was significantly lower than that in WT mice (Fig. 8A) ($P < 0.0001$; Fisher exact test), suggesting that the absence of GODZ reduces latency in the TG of HSV-1-infected mice.

We therefore tested whether the lower latency in the TG of HSV-1 strain McKrae-infected *GODZ*$^{-/-}$ mice was correlated with lower explant reactivation from latency. WT and *GODZ*$^{-/-}$ mice were ocularly infected with 2×10^5 PFU/eye of HSV-1 strain McKrae as described above, and virus reactivation was analyzed by explanting individual TG from infected mice on day 28 p.i., as described in Materials and Methods. Consistent with the lower LAT expression in the TG of GODZ$^{-/-}$ mice (Fig. 8A), the time to reactivation in GODZ$^{-/-}$ mice was longer than that for WT mice (Fig. 8B) (5.2 $\pm$ 0.2 days versus 4.6 $\pm$ 0.2 days; $P = 0.04$). Thus, in GODZ$^{-/-}$ mice, the time to explant reactivation was longer and correlated with the lower level of LAT RNA.

DISCUSSION

HSV-1 carries at least 85 genes, which are divided into two groups based on whether they are essential for virus replication *in vitro* (28). Both the gK and UL20 genes are considered essential genes for HSV-1 replication *in vitro* and *in vivo* (2–4, 29–32). We have reported previously that immunization of mice with HSV-1 gK exacerbates eye disease in ocularly infected mice (33, 34) and that recombinant viruses expressing two additional copies of HSV-1 gK exacerbate eye disease in ocularly infected mice (25). Notably, we have also found that HSV-1 gK binds to HSV-1 UL20 and that this interaction is required for transport of gK to the surface in infected cells (1, 2). Further analysis of the intracellular interactions of HSV-1 gK and UL20 have revealed that gK binds to signal peptide peptidase (SPP), an ER protein (35, 36), and that UL20 binds to GODZ, a Golgi apparatus protein (6). In those studies, we showed that either blockade of UL20 binding to GODZ or blockade of gK binding to SPP reduces HSV-1 infectivity, as well as gK and UL20 localization, respectively, *in vitro*. Thus, this network of interactions of UL20 with gK and UL20 and gK binding to GODZ and SPP, respectively, are essential for HSV-1 infectivity *in vitro*.

Further analysis of the interaction of UL20 with GODZ using two-hybrid systems and pulldown experiments confirmed that binding of UL20 to GODZ is indeed essential for viral replication *in vitro* (6). Moreover, we found that UL20 was palmitoylated by GODZ and that this palmitoylation is essential for HSV-1 infectivity (6). Either blocking of UL20 binding to GODZ using a GODZ dominant-negative mutant or blocking of palmitoylation of UL20 affected virus infectivity and localization of UL20 and gK *in vitro* (6). Previously, it was reported that HSV-1 UL51 is palmitoylated in the Golgi apparatus; however, no specific zinc finger protein that could possibly mediate the UL51 palmitoylation was identified, and the effect of this palmitoylation on virus infectivity was not determined (37). HSV-1 UL11 is also palmitoylated, but palmitoylation is not required for its function (38, 39). Glycoprotein N (gN) of human cytomegalovirus (HCMV) is palmitoylated, and its palmitoylation is essential for virus replication (40). However, no study has reported that HSV-1 gN (UL49.5) is palmitoylated, and even if it is palmitoylated, the absence of palmytoilation, in contrast to UL20, may not have any effects on virus infectivity, since HSV-1 gN-null mutant virus grew similarly to WT virus in tissue culture (41). In our previous study, we showed that GODZ binds to UL20 and does not bind to any other proteins of HSV-1 (6). As we did not detect GODZ binding to any HSV-1 protein other than UL20, the palmitoylation of UL11 and UL51 or any other possible palmitoylated gene(s) of HSV-1 may have been mediated by other members of the DHHC family. Finally, the complete absence of palmitoylation of UL20 in infected GODZ$^{-/-}$ MEFs suggests that palmitoylation of UL20 is GODZ dependent and is not facilitated by other members of the DHHC family.

Analysis of the roles of UL20 and its regulation *in vivo* are hampered by the essential role of UL20 and the inability of UL20 deletion mutants of HSV-1 to replicate efficiently *in vitro* or *in vivo* (3, 4, 32). Our recent construction of GODZ$^{-/-}$ mice (19), however, enabled investigation of the contribution of the GODZ component of the UL20-gK network to HSV-1 infectivity using MEFs derived from these mice, as well as *in vivo* analysis. In the current study, we demonstrate that HSV-1 replication in MEFs derived from GODZ$^{-/-}$ mice is markedly reduced compared with replication in MEFs from control WT mice. The complete absence of palmitoylation of UL20 in infected GODZ$^{-/-}$

MEFs confirmed our previous transfection studies showing that GODZ, but no other members of the DHHC family, is involved in palmitoylation of UL20 (6). Using several different strains of HSV-1, we examined the expression and localization of UL20, as well as proteins associated with three aspects of the virion structure, i.e., three different cell surface proteins (gB, gC, and gK), a tegument protein (VP22), and a capsid protein (VP26). The absence of GODZ had different effects on the cell surface proteins. The expression of gB was reduced, which could have been due to the effects of UL20 on gK, as suggested by our previous study showing that gK interacts with HSV-1 gB, in addition to UL20 (1, 42). The cell surface expression of gC, however, was not affected by the absence of GODZ. As expected, the absence of GODZ affected the localization and expression of both UL20 and gK, and this is consistent with our previous finding that blocking the interaction of gK with SPP affected virus replication and localization of gK in infected cells (36). The effects of the absence of GODZ were not restricted to the envelope proteins but also affected the expression of the tegument protein VP22 and the capsid protein VP26. No data are available on whether HSV-1 gB, gC, gK, VP22, or VP26 is palmitoylated. EM analysis revealed that the absence of GODZ was associated with entrapment of significant amounts of HSV-1 in the cytoplasm of the infected GODZ$^{-/-}$ MEFs, Furthermore, greater amounts of empty capsid were detected in the GODZ$^{-/-}$ MEFs. The EM analysis also revealed that the absence of GODZ caused signs of ER morphological stress, which could affect the maturation of the virions. It is possible that entrapment of gK in the ER in the absence of UL20 binding to GODZ contributes to ER stress, as we found previously that overexpression of gK caused physiological stress in the ER (36, 43, 44).

Analysis of the effects of the absence of GODZ on ocular virus replication *in vivo* using ocularly infected GODZ$^{-/-}$ mice indicated reduced replication in the cornea. We also detected different patterns of corneal infiltrates in infected GODZ$^{-/-}$ mice compared with WT controls. Following infection of *GODZ*$^{-/-}$ mice, low numbers of GFP^{+} HSV-1-infected cells, as well as low levels of UL20^{+} and gK^{+} infiltrates, were detected in corneas of infected mice (Fig. 2). In contrast, following ocular infection of WT mice, significantly higher numbers of GFP^{+} HSV-1-infected cells and higher levels of UL20^{+} and gK^{+} infiltrates were detected in the corneas of infected mice during primary infection. In this study, we also detected lower levels of UL20, gK, and gB transcripts in the corneas of infected *GODZ*$^{-/-}$ mice than in those of WT mice on day 5 p.i. In contrast, in the TG of infected *GODZ*$^{-/-}$ mice, we detected differences in UL20, but not gK or gB, expression. This discrepancy between the expression levels of viral transcripts in the TG and corneas of infected GODZ$^{-/-}$ mice could be due to tissue-specific viral gene expression affecting gB and gK, but not UL20.

The absence of GODZ in GODZ$^{-/-}$ mice did not affect the susceptibility of infected mice to ocular infection with virulent HSV-1 strain McKrae. Notably, however, mice lacking GODZ developed significantly less corneal scarring than the ocularly infected WT control mice. The presence of GODZ may possibly contribute to greater corneal scarring due to higher virus replication as a result of binding of UL20 to GODZ in infected mice, which would be consistent with our previous reports showing that there is a direct correlation of the virus load and the duration of primary virus replication in the eye with the severity of CS in ocularly infected WT mice (33, 45, 46). In the current study, we further found that the presence of GODZ, indirectly via binding to UL20 and not any immune dysfunction, contributes to the enhancement of latency in the TG of infected mice and that explant reactivation occurred more rapidly in infected WT mice than in their GODZ$^{-/-}$ counterparts. We have shown previously that the severity of corneal scaring is associated with higher latency in TG of latently infected mice (47). These data suggest a novel mechanism underlying establishment of latency and reactivation after ocular HSV-1 infection, which has potential clinical relevance, as higher latency is correlated with higher reactivation in individuals with ocular infection, and recurrent, rather than primary, infections are associated clinically with HSV-induced corneal scarring (48).

In the present study, we noted that virus infectivity in the eyes of ocularly infected

GODZ$^{-/-}$ mice, as well as virus replication in GODZ$^{-/-}$ MEFs, was reduced by 2- or 3-fold compared with WT mice. In contrast, we previously reported an at least 3-log-unit reduction in virus infectivity in mutant viruses lacking UL20 or gK (2–4, 29–32). We previously showed that GODZ and its most closely related paralog, SERZ-β, have indistinguishable substrate specificities *in vitro*; in contrast, *in vivo*, the two enzymes have distinct distributions in the Golgi complex (19, 49). While GODZ is highly restricted to the *cis*-Golgi network, SERZ-β is preferentially localized to the *trans*-Golgi network, and our previous results pointed to partial functional redundancy of GODZ and SERZ-β (19, 49). Thus, the smaller defects in virus replication seen in GODZ$^{-/-}$ cells than in experiments testing mutant viruses are likely due to compensation for loss of GODZ function by SERZ-β.

Collectively, our results suggest that GODZ plays an important role in viral replication and virus-associated pathogenesis through mechanisms associated with its interaction with UL20. As in this study, we previously reported that palmitoylation of UL20 is dependent on GODZ (6). Thus, binding of UL20 and its subsequent palmitoylation may be required for efficient primary virus replication, normal latency reactivation, and corneal scarring. Since UL20 is highly conserved among alphaherpesviruses, these findings may similarly apply to other members of the alphaherpesviruses, including HSV-2, pseudorabies virus (PRV), varicella-zoster virus (VZV), bovine herpesvirus 1 (BHV-1), and the gammaherpesvirus Marek's disease virus type 2 (MDV-2) (50–53). Thus, disruption of this interaction may not only be of interest for HSV-1 infection, but may also pertain to other members of the alphaherpesviruses.

MATERIALS AND METHODS

Cells, viruses, and mice. The RS cell line was generated from rabbit skin tissue, grown in minimal essential medium (MEM) plus 5% fetal bovine serum (FBS), and maintained and used as described previously (54). The generation of the VC1 virus with V5-tagged gK and the FLAG-tagged UL20 with an HSV-1 F background was performed in the Kousoulas laboratory as described previously (24). HSV-GFP$^+$ (a gift from Peter O'Hare, Marie Curie Research Institute, Surrey, United Kingdom) is a recombinant virus that contains the gene encoding a major tegument protein, VP22, linked to GFP (55, 56). The generation of YK608, a triply fluorescence-tagged virus expressing the capsid protein VP26 (yellow), the tegument protein VP22 (red), and the envelope protein gB (cyan) as fusion proteins, was described previously (27). Triple-plaque-purified HSV-1 strain McKrae, VC1 virus, HSV-GFP$^+$, and YK608 were grown in RS cell monolayers as described previously (33, 57). HSV-1 strain McKrae is a highly virulent strain of virus and infects mice efficiently without corneal scarification, whereas VC1, YK608, and HSV-GFP$^+$ are avirulent and required corneal scarification for efficient mouse ocular infection.

GODZ$^{-/-}$ mice were developed at Pennsylvania State University, as we described previously (19); rederived at Cedars-Sinai Medical Center; and backcrossed to C57BL/6 mice for six generations. WT C57BL/6 mice were used as controls and were purchased from The Jackson Laboratory (Bar Harbor, ME) and bred in-house at Cedars-Sinai Medical Center. Both male and female (6-week-old) mice were used in the study.

All animal procedures were performed in strict accordance with the Association for Research in Vision and Ophthalmology Statement for the Use of Animals in Ophthalmic and Vision Research (https://www.arvo.org/About/policies/statement-for-the-use-of-animals-in-ophthalmic-and-vision-research/) and the NIH *Guide for the Care and Use of Laboratory Animals* (64). The animal research protocol was approved by the Institutional Animal Care and Use Committee of Cedars-Sinai Medical Center (protocol no. 5374).

MEFs. On day 10 after establishment of pregnancy, embryos from WT and GODZ$^{-/-}$ mice were harvested, and the heads, placentas, and maternal tissues were removed. The embryos were then placed in a 10-cm plate with trypsin, cut into small pieces, and incubated at 37°C for 30 min. Trypsinization was then quenched by addition of Dulbecco's modified Eagle's medium (DMEM) with 10% fetal bovine serum (FBS) (Cellgro; Corning, Big Flats, NY), and the tissues were fragmented by pipetting 10 to 20 times. The cell suspensions were transferred to 10-cm dishes and cultured for 3 days in DMEM with 10% FBS.

Virus titration in MEFs. MEFs isolated from GODZ$^{-/-}$ and WT mice at 70 to 80% confluence were infected with McKrae virus at 0.01, 0.1, and 1 PFU/cell. Virus was harvested at the time points indicated by two cycles of freeze-thawing of the cell monolayers with medium. Virus titers were determined by standard plaque assays on RS cells as described previously (45).

Immunostaining of MEFs. MEFs (5×10^4 per well) were seeded in LabTek 4-chamber slides (Corning, Big Flats, NY) and infected with the following viruses: HSV-GFP$^+$ (0.1 and 1 PFU/cell for 24 h), VC1 (2 PFU/cell for 24 h), YK608 (2 PFU/cell for 16 h), and HSV-1 strain McKrae (0.1 and 1 PFU/cell for 24 h). Infection was synchronized on ice for 1 h. Cells infected with HSV-GFP$^+$ or YK608 were fixed with 4% paraformaldehyde, washed with 1× phosphate-buffered saline (PBS), and air dried. The HSV-GFP$^+$-infected cells were then mounted using 4′,6-diamidino-2-phenylindole (DAPI) (Prolong Gold; Invitrogen, Carlsbad, CA), while YK608-infected cells were mounted using Fluoromount aqueous mounting medium

(Sigma, St. Louis, MO). MEFs infected with VC1 virus were fixed with 4% paraformaldehyde, washed with 1× PBS, and then permeabilized with 0.3% Triton X-100 in PBS. The cells were then blocked using 1× sea blocker (Thermo Scientific, Rockford, IL) for 1 h at room temperature, washed 4 times with 1× PBS, and incubated with anti-FLAG (Genscript, Piscataway, NJ; catalog number A00187) to detect UL20 and anti-V5 (Bethyl Laboratories, Montgomery, TX; catalog number A190-119A) to detect gK or anti-FLAG and anti-GM130 (Abcam, Cambridge, MA; catalog number ab52649) antibodies. MEFs infected with HSV-1 strain McKrae were washed with cold PBS, fixed using 1:1 methanol-acetone at −20°C for 20 min, blocked using 1× sea blocker, and then incubated with anti-gC antibody (Genway, San Diego, CA; catalog number 20-251-401549) for 2 h. For live-cell staining, anti-V5 (for gK) antibody was added directly to VC1-infected cells, while for detection of gC, anti-gC antibody was added to McKrae-infected cells, and the cells were incubated for 30 min at 37°C. The cells were then washed three times in PBS, fixed using 4% paraformaldehyde, and incubated with the corresponding secondary antibodies for 2 h at room temperature. The slides were washed with PBS and mounted with Prolong Gold (Invitrogen). The fluorophores were imaged in separate channels by confocal microscopy using a Leica SP5-X confocal microscope, image acquisition, and data analysis system (Leica Microsystems, Buffalo Grove, IL).

EM of infected MEFs. MEFs were infected with 1 PFU/cell of McKrae virus for 24 h. The infected cells were then fixed with 2% glutaraldehyde-2% paraformaldehyde in 1× PBS for 1 h at room temperature and stored at 4°C until they were processed. The cells were washed with PBS and embedded in low-melting-point agarose. The agarose pellets were cut into small pieces and postfixed in 1% OsO_4 for 1 h at room temperature. The pellets were washed, dehydrated in a graded series of ethanol, treated with propylene oxide, and infiltrated with Eponate 12 (Ted Pella, Redding, CA) overnight. The cells were then embedded in fresh Eponate and polymerized at 60°C for 48 h. Approximately 50- to 60-nm-thick (silver-gray) sections were cut using an RMC MTX ultramicrotome and picked up on Formvar-coated copper grids. The sections were stained with saturated uranyl acetate and Reynolds lead citrate and examined using a JEOL 100CX electron microscope at 60 kV. Images were collected on type 4489 EM film, and the negatives were scanned to create digital files.

UL20 palmitoylation in GODZ$^{-/-}$ MEFs. MEFs from WT and GODZ$^{-/-}$ mice were infected with 1 PFU/cell of VC1 virus or mock infected for 24 h, and palmitoylation in infected cells was determined as we described recently (6). Briefly, the infected and mock-infected cells were lysed in lysis buffer as described above. The cell lysates were cleared and then incubated with anti-FLAG antibody overnight at 4°C. Protein A/G beads were added to the lysate as described above. After resuspension in LB buffer, one half was incubated with 1 M HAM (Sigma-Aldrich) and one half was incubated in the same buffer but without HAM as a control. After incubation for 1 h at room temperature, the beads were washed, incubated with 5 μm biotin-BMCC (Thermo Scientific, Asheville, NC), washed again, and incubated in 2× lithium dodecyl sulfate (LDS) buffer (Life Technologies, Carlsbad, CA) for 10 min at 80°C as described above. The eluted samples were subjected to SDS-PAGE and then transferred to a polyvinylidene difluoride (PVDF) membrane. The palmitoylation signal was assessed using HRP-conjugated streptavidin to detect the biotin label. The level of UL20 protein for each treatment was assessed by Western blotting using anti-FLAG antibody and HRP-conjugated anti-mouse secondary antibody.

Ocular infection. GODZ$^{-/-}$ and WT C57BL/6 control mice were infected ocularly with 2×10^5 PFU of HSV-1 strain McKrae per eye in 2 μl of tissue culture medium as an eye drop without corneal scarification, as we described previously (45, 46). In some experiments, mice were infected with 2×10^5 PFU/eye of HSV-GFP$^+$ or VC1 virus with corneal scarification as described previously (58).

Evaluation of CS. The severity of corneal scarring in surviving mice on day 28 p.i. was scored in a masked fashion by examination with a slit lamp biomicroscope following addition of 1% fluorescein eye drops. Disease was scored on a scale of 0 to 4 (0, no disease; 1, 25% involvement; 2, 50% involvement; 3, 75% involvement; and 4, 100% involvement).

Isolation of RNA from corneas and TG of infected mice. GODZ$^{-/-}$ and WT C57BL/6 mice were ocularly infected with 2×10^5 PFU/eye of HSV-1 strain McKrae. Corneas and TG from infected mice were collected on days 3, 5, and 7 p.i. Isolated tissues were immersed in RNAlater RNA stabilization reagent (Qiagen, Germantown, MD) and stored at −80°C until they were processed. The corneas or TG from each animal were processed for RNA extraction using TRIzol reagent as we described previously (59). Isolated total RNA was reverse transcribed with random-hexamer primers and murine leukemia virus (MuLV) reverse transcriptase provided in the High Capacity cDNA reverse transcription kit (Applied Biosystems, Foster City, CA) according to the manufacturer's recommendations. All isolated corneas were free of contamination from other parts of the mouse eye, vitreous fluid, and tears.

Titration of virus in tears. Tear films were collected from both eyes of 20 mice per group on days 1 to 7 p.i. using a Dacron-tipped swab. Each swab was placed in tissue culture medium (1 ml), and the amount of virus in the medium was determined by a standard plaque assay on RS cells (60).

Detection of GFP expression in whole corneas of infected mice. Mice were ocularly infected with 2×10^5 PFU/eye of HSV-GFP$^+$ virus. On days 4 and 7 p.i., mice were euthanized, and their eyeballs were removed and fixed in 4% paraformaldehyde for 2 h at room temperature. The corneal tissue was separated, and the tissues were flattened with four partial cuts from the limbal to central cornea. The corneal tissue was mounted with Vectashield medium containing DAPI (Vector Laboratories, Burlingame, CA) as described previously (61). Images were acquired as described above.

Detection of gK and UL2 in corneas of infected mice. Mice were ocularly infected with VC1 virus. Eyeballs from infected mice were removed at autopsy on day 5 p.i. and placed in Tissue-TeK OCT embedding medium (SaKura Fintek, Torrance, CA), frozen using dry ice, and then stored at −80°C. The frozen tissue was sectioned at 10-μm thickness using a Leica CM1950, and the sections were placed on slides and fixed using Pen Fix (Thermo Scientific) with 1:60 (vol/vol) glacial acetic acid. The tissue sections

were then washed with 1× PBS, blocked with sea blocking buffer with 3% donkey serum (Vector Laboratories, Burlingame, CA), incubated with anti-FLAG (for UL20) and anti-V5 (for gK) antibodies, washed, and then reacted with Alexa Fluor 488- and Alexa Fluor 647-conjugated secondary antibodies, respectively. Images were acquired by confocal microscopy as described above.

TaqMan real-time PCR and PCR. The gB, gK, UL20, and LAT custom-made sets of primers and probes used in this study were as follows: (i) gB-specific primers, forward (5′-AACGCGACGCACATCAAG-3′) and reverse (5′-CTGGTACGCGATCAGAAAGC-3′), and probe (5′-6-carboxyfluorescein [FAM]-CAGCCG CAGTACTACC-3′); (ii) gK-specific primers, forward (5′-GGCCACCTACCTCTTGAACTAC-3′) and reverse (5′-CAGGCGGGTAATTTTCGTGTAG-3′), and probe (5′-FAM-CAGGCCGCATCGTATC-3′); amplicon length, 82 bp; (iii) UL20-specific primers, forward (5′-CCATCGTCGGCTACTACGTTAC-3′) and reverse (5′-CGATCCCT CTTGATGTTAACGTACA-3′), and probe (5′-FAM-CCCGCACCGCCCAC-3′; amplicon length, 70 bp); and (iv) LAT-specific primers, forward (5′-GGGTGGGCTCGTGTTACAG-3′) and reverse (5′-GGACGGGTAAGTAACA GAGTCTCTA-3′), and probe (5′-FAM-ACACCAGCCCGTTCTTT-3′; amplicon length, 81 bp). As an internal control, a set of GAPDH primers from Applied Biosystems (assay identifier [ID], m999999.15_G1; amplicon length, 107 bp) was used.

The expression levels of gB, gK, UL20, and LAT, as well as the expression of the endogenous control GAPDH gene, were evaluated using a commercially available TaqMan gene expression assay kit (Applied Biosystems, Foster City, CA) containing optimized primer and probe concentrations. In each experiment, estimated relative copy numbers for gB, gK, UL20, and LAT were calculated using standard curves generated from pAc-gB1 (for gB), pGem-gK1040 (for gK), pcDNA-UL20 (for UL20), and pGem-LAT5300 (for LAT). Briefly, each plasmid DNA template was serially diluted 10-fold so that 5 μl contained from 10^3 to 10^{11} copies of the desired gene and then subjected to TaqMan PCR with the same set of primers as the test samples. By comparing the normalized threshold cycle (C_T) of each sample to the threshold cycle of the standards, the copy number for each reaction was determined. qPCR and qRT-PCR were performed using an ABI ViiA7 sequence detection system (Applied Biosystems, Foster City, CA) in 384-well plates. The C_T values, which represent the PCR cycles at which there is a noticeable increase in the reporter fluorescence above baseline, were determined using ViiA7 RUO software.

***In vitro* explant reactivation assay.** Mice were sacrificed at 28 days p.i., and individual TG were removed and cultured in 1.5 ml tissue culture medium, as we described previously (62). Briefly, a 100-μl aliquot was removed from each culture daily for 15 days and used to infect RS cell monolayers. The RS cells were monitored daily for the appearance of cytopathic effect (CPE) for 5 days to determine the time of first appearance of reactivated virus from each TG. As the media from the explanted TG cultures were plated daily, the time at which reactivated virus first appeared in the explanted TG cultures could be determined.

Statistical analyses. The Student *t* test and Fisher exact test were performed using the computer program Instat (GraphPad, San Diego, CA). Results were considered statistically significant when the *P* value was <0.05.

SUPPLEMENTAL MATERIAL

Supplemental material for this article may be found at https://doi.org/10.1128/JVI.01599-17.

SUPPLEMENTAL FILE 1, PDF file, 0.1 MB.

REFERENCES

1. Foster TP, Chouljenko VN, Kousoulas KG. 2008. Functional and physical interactions of the herpes simplex virus type 1 UL20 membrane protein with glycoprotein K. J Virol 82:6310–6323. https://doi.org/10.1128/JVI.00147-08.
2. Foster TP, Melancon JM, Baines JD, Kousoulas KG. 2004. The herpes simplex virus type 1 UL20 protein modulates membrane fusion events during cytoplasmic virion morphogenesis and virus-induced cell fusion. J Virol 78:5347–5357. https://doi.org/10.1128/JVI.78.10.5347-5357.2004.
3. Foster TP, Kousoulas KG. 1999. Genetic analysis of the role of herpes simplex virus type 1 glycoprotein K in infectious virus production and egress. J Virol 73:8457–8468.
4. Baines JD, Ward PL, Campadelli-Fiume G, Roizman B. 1991. The UL20 gene of herpes simplex virus 1 encodes a function necessary for viral egress. J Virol 65:6414–6424.
5. Agelidis AM, Shukla D. 2015. Cell entry mechanisms of HSV: what we have learned in recent years. Future Virol 10:1145–1154. https://doi.org/10.2217/fvl.15.85.
6. Wang S, Mott KR, Wawrowsky K, Kousoulas KG, Luscher B, Ghiasi H. 2017. Binding of HSV-1 UL20 to GODZ affects its palmitoylation and is essential for infectivity and proper targeting and localization of UL20 and gK. J Virol 91:e00945-17. https://doi.org/10.1128/JVI.00945-17.
7. Linder ME, Deschenes RJ. 2007. Palmitoylation: policing protein stability and traffic. Nat Rev Mol Cell Biol 8:74–84. https://doi.org/10.1038/nrm2084.
8. Fukata Y, Fukata M. 2010. Protein palmitoylation in neuronal development and synaptic plasticity. Nat Rev Neurosci 11:161–175. https://doi.org/10.1038/nrn2788.
9. Greaves J, Chamberlain LH. 2011. DHHC palmitoyl transferases: substrate interactions and (patho)physiology. Trends Biochem Sci 36:245–253. https://doi.org/10.1016/j.tibs.2011.01.003.
10. Mitchell DA, Vasudevan A, Linder ME, Deschenes RJ. 2006. Protein palmitoylation by a family of DHHC protein S-acyltransferases. J Lipid Res 47:1118–1127. https://doi.org/10.1194/jlr.R600007-JLR200.
11. Batistic O. 2012. Genomics and localization of the Arabidopsis DHHC-cysteine-rich domain S-acyltransferase protein family. Plant Physiol 160:1597–1612. https://doi.org/10.1104/pp.112.203968.
12. Uemura T, Mori H, Mishina M. 2002. Isolation and characterization of Golgi apparatus-specific GODZ with the DHHC zinc finger domain. Biochem Biophys Res Commun 296:492–496. https://doi.org/10.1016/S0006-291X(02)00900-2.
13. Korycka J, Lach A, Heger E, Boguslawska DM, Wolny M, Toporkiewicz M, Augoff K, Korzeniewski J, Sikorski AF. 2012. Human DHHC proteins: a spotlight on the hidden player of palmitoylation. Eur J Cell Biol 91:107–117. https://doi.org/10.1016/j.ejcb.2011.09.013.
14. Roth AF, Wan J, Bailey AO, Sun B, Kuchar JA, Green WN, Phinney BS, Yates JR III, Davis NG. 2006. Global analysis of protein palmitoylation in yeast. Cell 125:1003–1013. https://doi.org/10.1016/j.cell.2006.03.042.
15. Resh MD. 1999. Fatty acylation of proteins: new insights into membrane

targeting of myristoylated and palmitoylated proteins. Biochim Biophys Acta 1451:1–16. https://doi.org/10.1016/S0167-4889(99)00075-0.
16. Smotrys JE, Linder ME. 2004. Palmitoylation of intracellular signaling proteins: regulation and function. Annu Rev Biochem 73:559–587. https://doi.org/10.1146/annurev.biochem.73.011303.073954.
17. Greaves J, Chamberlain LH. 2007. Palmitoylation-dependent protein sorting. J Cell Biol 176:249–254. https://doi.org/10.1083/jcb.200610151.
18. Keller CA, Yuan X, Panzanelli P, Martin ML, Alldred M, Sassoe-Pognetto M, Luscher B. 2004. The gamma2 subunit of GABA(A) receptors is a substrate for palmitoylation by GODZ. J Neurosci 24:5881–5891. https://doi.org/10.1523/JNEUROSCI.1037-04.2004.
19. Kilpatrick CL, Murakami S, Feng M, Wu X, Lal R, Chen G, Du K, Luscher B. 2016. Dissociation of Golgi-associated DHHC-type zinc finger protein (GODZ)- and Sertoli cell gene with a zinc finger domain-beta (SERZ-beta)-mediated palmitoylation by loss of function analyses in knock-out mice. J Biol Chem 291:27371–27386. https://doi.org/10.1074/jbc.M116.732768.
20. Fang C, Deng L, Keller CA, Fukata M, Fukata Y, Chen G, Luscher B. 2006. GODZ-mediated palmitoylation of GABA(A) receptors is required for normal assembly and function of GABAergic inhibitory synapses. J Neurosci 26:12758–12768. https://doi.org/10.1523/JNEUROSCI.4214-06.2006.
21. Fukata M, Fukata Y, Adesnik H, Nicoll RA, Bredt DS. 2004. Identification of PSD-95 palmitoylating enzymes. Neuron 44:987–996. https://doi.org/10.1016/j.neuron.2004.12.005.
22. Sharma C, Rabinovitz I, Hemler ME. 2012. Palmitoylation by DHHC3 is critical for the function, expression, and stability of integrin alpha6beta4. Cell Mol Life Sci 69:2233–2244. https://doi.org/10.1007/s00018-012-0924-6.
23. Foster TP, Melancon JM, Olivier TL, Kousoulas KG. 2004. Herpes simplex virus type 1 glycoprotein K and the UL20 protein are interdependent for intracellular trafficking and trans-Golgi network localization. J Virol 78:13262–13277. https://doi.org/10.1128/JVI.78.23.13262-13277.2004.
24. Jambunathan N, Chowdhury S, Subramanian R, Chouljenko VN, Walker JD, Kousoulas KG. 2011. Site-specific proteolytic cleavage of the amino terminus of herpes simplex virus glycoprotein K on virion particles inhibits virus entry. J Virol 85:12910–12918. https://doi.org/10.1128/JVI.06268-11.
25. Matundan HH, Mott KR, Akhtar AA, Breunig JJ, Ghiasi H. 2015. Mutations within the pathogenic region of herpes simplex virus 1 gK signal sequences alter cell surface expression and neurovirulence. J Virol 89:2530–2542. https://doi.org/10.1128/JVI.03506-14.
26. Mettenleiter TC, Klupp BG, Granzow H. 2009. Herpesvirus assembly: an update. Virus Res 143:222–234. https://doi.org/10.1016/j.virusres.2009.03.018.
27. Sugimoto K, Uema M, Sagara H, Tanaka M, Sata T, Hashimoto Y, Kawaguchi Y. 2008. Simultaneous tracking of capsid, tegument, and envelope protein localization in living cells infected with triply fluorescent herpes simplex virus 1. J Virol 82:5198–5211. https://doi.org/10.1128/JVI.02681-07.
28. McGeoch DJ, Dalrymple MA, Davison AJ, Dolan A, Frame MC, McNab D, Perry LJ, Scott JE, Taylor P. 1988. The complete DNA sequence of the long unique region in the genome of herpes simplex virus type 1. J Gen Virol 69:1531–1574. https://doi.org/10.1099/0022-1317-69-7-1531.
29. Hutchinson L, Johnson DC. 1995. Herpes simplex virus glycoprotein K promotes egress of virus particles. J Virol 69:5401–5413.
30. Hutchinson L, Roop-Beauchamp C, Johnson DC. 1995. Herpes simplex virus glycoprotein K is known to influence fusion of infected cells, yet is not on the cell surface. J Virol 69:4556–4563.
31. David AT, Baghian A, Foster TP, Chouljenko VN, Kousoulas KG. 2008. The herpes simplex virus type 1 (HSV-1) glycoprotein K (gK) is essential for viral corneal spread and neuroinvasiveness. Curr Eye Res 33:455–467. https://doi.org/10.1080/02713680802130362.
32. Jayachandra S, Baghian A, Kousoulas KG. 1997. Herpes simplex virus type 1 glycoprotein K is not essential for infectious virus production in actively replicating cells but is required for efficient envelopment and translocation of infectious virions from the cytoplasm to the extracellular space. J Virol 71:5012–5024.
33. Ghiasi H, Slanina S, Nesburn AB, Wechsler SL. 1994. Characterization of baculovirus-expressed herpes simplex virus type 1 glycoprotein K. J Virol 68:2347–2354.
34. Ghiasi H, Cai S, Slanina S, Nesburn AB, Wechsler SL. 1997. Nonneutralizing antibody against the glycoprotein K of herpes simplex virus type-1 exacerbates herpes simplex virus type-1-induced corneal scarring in various virus-mouse strain combinations. Invest Ophthalmol Vis Sci 38:1213–1221.
35. Allen SJ, Mott KR, Ghiasi H. 2014. Inhibitors of signal peptide peptidase (SPP) affect HSV-1 infectivity in vitro and in vivo. Exp Eye Res 123:8–15. https://doi.org/10.1016/j.exer.2014.04.004.
36. Allen SJ, Mott KR, Matsuura Y, Moriishi K, Kousoulas KG, Ghiasi H. 2014. Binding of HSV-1 glycoprotein K (gK) to signal peptide peptidase (SPP) is required for virus infectivity. PLoS One 9:e85360. https://doi.org/10.1371/journal.pone.0085360.
37. Nozawa N, Daikoku T, Koshizuka T, Yamauchi Y, Yoshikawa T, Nishiyama Y. 2003. Subcellular localization of herpes simplex virus type 1 UL51 protein and role of palmitoylation in Golgi apparatus targeting. J Virol 77:3204–3216. https://doi.org/10.1128/JVI.77.5.3204-3216.2003.
38. Koshizuka T, Kawaguchi Y, Nozawa N, Mori I, Nishiyama Y. 2007. Herpes simplex virus protein UL11 but not UL51 is associated with lipid rafts. Virus Genes 35:571–575. https://doi.org/10.1007/s11262-007-0156-2.
39. Baird NL, Starkey JL, Hughes DJ, Wills JW. 2010. Myristylation and palmitylation of HSV-1 UL11 are not essential for its function. Virology 397:80–88. https://doi.org/10.1016/j.virol.2009.10.046.
40. Mach M, Osinski K, Kropff B, Schloetzer-Schrehardt U, Krzyzaniak M, Britt W. 2007. The carboxy-terminal domain of glycoprotein N of human cytomegalovirus is required for virion morphogenesis. J Virol 81:5212–5224. https://doi.org/10.1128/JVI.01463-06.
41. Striebinger H, Funk C, Raschbichler V, Bailer SM. 2016. Subcellular trafficking and functional relationship of the HSV-1 glycoproteins N and M. Viruses 8:83. https://doi.org/10.3390/v8030083.
42. Chouljenko VN, Iyer AV, Chowdhury S, Kim J, Kousoulas KG. 2010. The herpes simplex virus type 1 UL20 protein and the amino terminus of glycoprotein K (gK) physically interact with gB. J Virol 84:8596–8606. https://doi.org/10.1128/JVI.00298-10.
43. Foster TP, Rybachuk GV, Alvarez X, Borkhsenious O, Kousoulas KG. 2003. Overexpression of gK in gK-transformed cells collapses the Golgi apparatus into the endoplasmic reticulum inhibiting virion egress, glycoprotein transport, and virus-induced cell fusion. Virology 317:237–252. https://doi.org/10.1016/j.virol.2003.07.008.
44. Mott KR, Perng GC, Osorio Y, Kousoulas KG, Ghiasi H. 2007. A recombinant herpes simplex virus type 1 expressing two additional copies of gK is more pathogenic than wild-type virus in two different strains of mice. J Virol 81:12962–12972. https://doi.org/10.1128/JVI.01442-07.
45. Ghiasi H, Kaiwar R, Nesburn AB, Slanina S, Wechsler SL. 1994. Expression of seven herpes simplex virus type 1 glycoproteins (gB, gC, gD, gE, gG, gH, and gI): comparative protection against lethal challenge in mice. J Virol 68:2118–2126.
46. Ghiasi H, Bahri S, Nesburn AB, Wechsler SL. 1995. Protection against herpes simplex virus-induced eye disease after vaccination with seven individually expressed herpes simplex virus 1 glycoproteins. Invest Ophthalmol Vis Sci 36:1352–1360.
47. Mott KR, Bresee CJ, Allen SJ, Ben Mohamed L, Wechsler SL, Ghiasi H. 2009. Level of herpes simplex virus type 1 latency correlates with severity of corneal scarring and exhaustion of CD8+ T cells in trigeminal ganglia of latently infected mice. J Virol 83:2246–2254. https://doi.org/10.1128/JVI.02234-08.
48. Liesegang TJ. 1999. Classification of herpes simplex virus keratitis and anterior uveitis. Cornea 18:127–143. https://doi.org/10.1097/00003226-199903000-00001.
49. Du K, Murakami S, Sun Y, Kilpatrick C, Luscher B. 2017. DHHC7 palmitoylates Glut4 and regulates Glut4 membrane translocation. J Biol Chem 292:2979–2991. https://doi.org/10.1074/jbc.M116.747139.
50. Klupp BG, Kern H, Mettenleiter TC. 1992. The virulence-determining genomic BamHI fragment 4 of pseudorabies virus contains genes corresponding to the UL15 (partial), UL18, UL19, UL20, and UL21 genes of herpes simplex virus and a putative origin of replication. Virology 191:900–908. https://doi.org/10.1016/0042-6822(92)90265-Q.
51. Davison AJ, Scott JE. 1986. The complete DNA sequence of varicella-zoster virus. J Gen Virol 67:1759–1816. https://doi.org/10.1099/0022-1317-67-9-1759.
52. Vlcek C, Benes V, Lu Z, Kutish GF, Paces V, Rock D, Letchworth GJ, Schwyzer M. 1995. Nucleotide sequence analysis of a 30-kb region of the bovine herpesvirus 1 genome which exhibits a colinear gene arrangement with the UL21 to UL4 genes of herpes simplex virus. Virology 210:100–108. https://doi.org/10.1006/viro.1995.1321.
53. Hatama S, Jang HK, Izumiya Y, Cai JS, Tsushima Y, Kato K, Miyazawa T, Kai C, Takahashi E, Mikami T. 1999. Identification and DNA sequence analysis of the Marek's disease virus serotype 2 genes homologous to the herpes

simplex virus type 1 UL20 and UL21. J Vet Med Sci 61:587–593. https://doi.org/10.1292/jvms.61.587.
54. Perng GC, Dunkel EC, Geary PA, Slanina SM, Ghiasi H, Kaiwar R, Nesburn AB, Wechsler SL. 1994. The latency-associated transcript gene of herpes simplex virus type 1 (HSV-1) is required for efficient in vivo spontaneous reactivation of HSV-1 from latency. J Virol 68:8045–8055.
55. Elliott G, O'Hare P. 1999. Intercellular trafficking of VP22-GFP fusion proteins. Gene Ther 6:149–151. https://doi.org/10.1038/sj.gt.3300850.
56. Elliott G, O'Hare P. 1999. Live-cell analysis of a green fluorescent protein-tagged herpes simplex virus infection. J Virol 73:4110–4119.
57. Allen SJ, Mott KR, Ghiasi H. 2014. Overexpression of herpes simplex virus glycoprotein K (gK) alters expression of HSV receptors in ocularly-infected mice. Invest Ophthalmol Vis Sci 55:2442–2451. https://doi.org/10.1167/iovs.14-14013.
58. BenMohamed L, Osorio N, Khan AA, Srivastava R, Huang L, Krochmal JJ, Garcia JM, Simpson JL, Wechsler SL. 2016. Prior corneal scarification and injection of immune serum are not required before ocular HSV-1 infection for UV-B-induced virus reactivation and recurrent herpetic corneal disease in latently infected mice. Curr Eye Res 41:747–756. https://doi.org/10.3109/02713683.2015.1061024.
59. Matundan H, Mott KR, Ghiasi H. 2014. Role of CD8+ T cells and myeloid DCs in protection from ocular HSV-1 challenge in immunized mice. J Virol 88:8016–8027. https://doi.org/10.1128/JVI.00913-14.
60. Ghiasi H, Cai S, Slanina SM, Perng GC, Nesburn AB, Wechsler SL. 1999. The role of interleukin (IL)-2 and IL-4 in herpes simplex virus type 1 ocular replication and eye disease. J Infect Dis 179:1086–1093. https://doi.org/10.1086/314736.
61. Gaddipati S, Rao P, Jerome AD, Burugula BB, Gerard NP, Suvas S. 2016. Loss of neurokinin-1 receptor alters ocular surface homeostasis and promotes an early development of herpes stromal keratitis. J Immunol 197:4021–4033. https://doi.org/10.4049/jimmunol.1600836.
62. Mott KR, Ghiasi H. 2008. Role of dendritic cells in enhancement of herpes simplex virus type 1 latency and reactivation in vaccinated mice. Clin Vaccine Immunol 15:1859–1867. https://doi.org/10.1128/CVI.00318-08.
63. Ghiasi H, Kaiwar R, Nesburn AB, Wechsler SL. 1992. Expression of herpes simplex virus type 1 glycoprotein B in insect cells. Initial analysis of its biochemical and immunological properties. Virus Res 22:25–39.
64. National Research Council. 2011. Guide for the care and use of laboratory animals, 8th ed. National Academies Press, Washington, DC.